Rho Transcription Factor: Symmetry and Binding of Bicyclomycin†

Fabien Vincent,‡ Matthew Openshaw,§ Mark Trautwein,§ Simon J. Gaskell,*,§ Harold Kohn,*,|| and William R. Widger*,⊥

Department of Chemistry, University of Houston, Houston, Texas 77204-5641, Michael Barber Centre for Mass Spectrometry, Department of Chemistry, UMIST, P.O. Box 88, Manchester M60 1 QD, United Kingdom, Division of Medicinal Chemistry and Natural Products, School of Pharmacy, University of North Carolina at Chapel Hill, Chapel Hill, North Carolina 27599-7360, and Department of Biology and Biochemistry, University of Houston, Houston, Texas 77204-5934

Received March 6, 2000; Revised Manuscript Received June 1, 2000

ABSTRACT: The antibiotic bicyclomycin inhibits rho-dependent termination processes by interfering with RNA translocation by preventing RNA binding at the translocation site or by uncoupling the translocation process from ATP hydrolysis. Previous studies have shown that bicyclomycin binds near the ATP hydrolysis pocket on rho. The hexameric structure of rho indicates that it is in a class of enzymes with strong sequence similarity to F_1-ATP synthase. The bicyclomycin derivative 5a-formylbicyclomycin, an inhibitor comparable to bicyclomycin, was previously shown to form a stable imine with rho and when reduced to the amine with $NaBH_4$ to singly label five of the six rho subunits. Lysine-336 was identified by mass spectrometric analysis of trypsin-digested fragments as the site of 5a-formylbicyclomycin adduction. A model of rho was made by threading the rho sequence on the known crystal structure of the α and β subunits of F_1-ATP synthase. The model, along with information concerning the extent and site of 5a-formylbicyclomycin adduction, indicates an overall C6 symmetry for rho subunit organization. We propose that the sequence similarity between rho and F_1-ATP synthase extends to a similar quaternary structure and an equivalent enzyme mechanism. The proposed mechanism of RNA translocation coupled with ATP hydrolysis changes the overall symmetry of rho from C6 to C6/C3.

Rho-dependent transcription termination can regulate gene expression by controlling termination or antitermination events just downstream of *rut* sites located either upstream of genes or between cistrons that are within operons (*1*, *2*) (see reviews in refs *3* and *4*). Rho affords transcriptional regulation that can be modified with various antitermination factors. Rho is crucial for Gram-negative cell viability and *Escherichia coli* bearing temperature-sensitive rho mutations are lethal above a permissible temperature (*5*−*7*).

Rho is a hexamer of 47 kDa identical subunits (*8*) arranged in a toroidal shape (*9*−*11*) but controversy remains as to the symmetry of the hexameric assembly. Evidence has been presented that rho subunit symmetry is either D3 (*12*) or C6/C3 (*13*). Molecular recognition of newly synthesized RNA by rho at specific *rut* sites proceeds through tight or primary RNA binding sites (*14*). Although rho monomers appear to be in an equilibrium with the dimer, the tetramer and the hexamer, binding ATP and or RNA favors the assembly of the hexamer (*15*−*18*). ATP hydrolysis used by rho to track 5′ to 3′ toward the stalled RNA polymerase is activated by RNA binding at a secondary binding site (for reviews, see refs *3* and *4*). The two RNA binding sites lead to a tethered-tracking model for rho action (*19*, *20*). The transcript dissociates from the polymerase when rho encounters the polymerase possibly by a rho helicase activity, and presumably, rho is freed from the RNA by subunit dissociation (*21*). Transcription termination by rho is kinetically coupled to the polymerase (*22*), and correct termination depends on the velocity by which both rho and the polymerase move along the RNA and DNA, respectively. Termination occurs when polymerase rates are slower than the rate of rho translocation. Antitermination occurs when the translocation rate of rho is slower than the polymerization rate of RNA (*23*).

Rho possesses three tight and three weak ATP binding sites possibly located on alternating subunits (*24*−*26*). The tight sites bind ATP with a 10-fold lower K_d relative to the enzymatic K_M values for ATP (*27*). The catalytic ATP binding sites are thought to alternate with the tighter binding, noncatalytic sites and implies a C3 or a D3 symmetry for rho subunit organization (*12*, *28*). Several models of rho quaternary structure have been proposed, each concerned with the directionality of RNA binding among subunits (*12*, *13*, *27*) and the heterogeneity of ATP binding (*24*−*26*). Rho factor shows considerable sequence and predicted secondary

† The work was supported by the U.S. Public Health Service National Institutes of Health Grant GM37934, the Robert A. Welch Foundation (Grants E607, H.K.; E1381, W.R.W.), The Higher Education Funding Council for England (Joint Research Equipment Initiative, S.J.G.) and the Trustees of the Analytical Chemistry Trust Fund of the Royal Society of Chemistry (SAC Studentship, M.O.).

* To whom correspondence should be addressed. (S.J.G.) Phone: 44-161-2004474. Fax: 44-161-200-4421. E-mail: simon.gaskell@umist.ac.uk. (H.K.) Phone: (919) 966-2680. Fax: (919) 843-7835. E-mail: harold_kohn@unc.edu. (W.RW.) Phone: (713) 743-8368. Fax: (713) 743-8351. E-mail: widger@uh.edu.

‡ Department of Chemistry, University of Houston. Present address: Genomics Institute of the Novartis Foundation, 3115 Merryfield Row, San Diego, CA 92121.

§ Michael Barber Centre for Mass Spectrometry.

|| Division of Medicinal Chemistry and Natural Products, School of Pharmacy, University of North Carolina at Chapel Hill.

⊥ Department of Biology and Biochemistry, University of Houston.

10.1021/bi000504+ CCC: $19.00
Published on Web 07/15/2000

structure similarity to the β-subunit of F_1-ATP synthase, and models of rho based on this structure have been presented (*12*, *29*−*32*). The primary RNA binding site has been located at N-terminal residues 1−151 with a conserved RNA binding locus, GPN-1, a GFGFLR motif located at position 61−66 (*14*, *33*). A crystal structure for the N-terminal 130 residues has been solved (*34*) along with an NMR[1] solution structure (*35*). An ATP binding domain and hydrolysis pocket have been proposed based upon the sequence similarity between rho and the F_1-ATP synthase (*29*). The secondary RNA binding domain has not been directly identified. However, mutations in rho affecting the secondary binding of RNA (*30*, *36*) indicate this site maybe located within the central hole of the toroid ring suggesting RNA tracks through the central hole of the enzyme (*31*). Recently, presteady-state kinetics indicate that ATP hydrolysis proceeds sequentially from one catalytic subunit to another (*25*). The sequence similarity between rho and F_1-ATP synthase suggests both a tertiary and quaternary similarity and, possibly, an equivalent enzyme mechanism (*30*).

Bicyclomycin (**1**) has been shown to inhibit rho by a reversible, noncompetitive pathway with respect to ATP (*37*). Transcription termination measured in vitro suggests bicyclomycin slows down rho translocation resulting in longer transcripts (*23*). This is accomplished by either competing with RNA binding at the secondary site or uncoupling ATP hydrolysis from translocation or by both. The approximate location of the bicyclomycin binding site was predicted from the positions of mutated amino acids yielding bicyclomycin-resistant rho proteins and from a structural model of the rho monomer built from the crystal structure of the β-subunit of F_1-ATP synthase (subunit F) (*32*). Mutations S266A (*38*), M219K (*38*), and D210G (*39*) place the bicyclomycin binding at or near the catalytic pocket of ATP hydrolysis. Further supporting this notion was the identification of K181 as the site of modification of bicyclomycin affinity label 5a-(3-formylanilino)dihydrobicyclomycin (**2**) (*40*). However, one bicyclomycin-resistant mutation, G337S (*38*), does not fit this model. This residue maps to the subunit's *opposite* face of the F_1-ATP synthase model. To better understand the relationship of G337S to our previous model of rho (*32*), a revised model has been generated in which the rho sequence was threaded upon both the α and β subunits of F_1-ATP synthase. The gaps between rho and F_1-ATP synthase sequences were corrected. We show the covalent modification of K336 with 5a-formylbicyclomycin (**3**) after $NaBH_4$ reduction and report on the implications of this finding for the quaternary structure of rho.

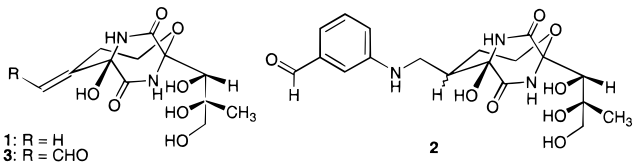

METHODS AND MATERIALS

General Procedure for Reductive Amination of Rho by 5a-Formylbicyclomycin (3) GP-1. A solution (0.2 mL) containing ATPase buffer (40 mM Tris·HCl, pH 7.9, 50 mM KCl, 12 mM $MgCl_2$, 0.1 mM EDTA, 0.1 mM DTT) with 1 μM rho, 1 mM ATP, 40 nM poly C, and 40 mM **3** was incubated at 25 °C for 4 h. A 20 μL sample of an aqueous 600 mM solution of $NaBH_4$ was added, and the reaction was allowed to stand at 25 °C for 20 min. The reaction mixture was dialyzed at 4 °C for 20 h against 100 mM NaCl, 10 mM Tris·HCl, pH 7.6, 5% glycerol, 0.1 mM EDTA, and 0.1 mM DTT. The percentage of rho inactivation was determined by measuring the initial velocity of ATPase activity using previously published procedures (*37*) and adding 40 nM poly C, 250 mM ATP, and 0.5 mCi [γ-^{32}P]ATP.

Partial Trypsin Digestion. The reductive amination of rho (3 μM) was conducted using general procedure GP-1 in the presence of poly C (120 nM) and ATP (3 mM). The samples were stored in dialysis buffer at room temperature. A portion (100 μL) was incubated with 1.5 μL of poly C (1 mg/mL in water), 1.5 μL of ATP solution (10 mM in ATPase buffer), and 1.5 μL freshly prepared trypsin solution (0.1 mg/mL in ATPase buffer). Digestion was allowed to proceed at 37 °C for 30 min before being terminated by additing 0.5% volume of formic acid. The products of digestion were desalted using a "Protein Micro Trap" cartridge (Michrom BioResources, Inc., Auburn, CA) with elution in acetonitrile/water (80/20, v/v, incorporating 0.1% formic acid).

Complete Trypsin Digestion. Rho protein (3 μM) was incubated with **3** (400 μM) in the presence of poly C (120 nM) and ATP (3 mM), as described in GP-1. The product of the reaction was subjected to dialysis (4 °C, 20 h) against 100 mM NaCl, 10 mM Tris·HCl (pH 7.6), 5% glycerol, 0.1 mM EDTA, and 0.1 mM DTT. A portion of the dialysate (corresponding to 19 μg of protein) was treated with a solution of trypsin in 2 mM $CaCl_2$ to give an enzyme/substrate ratio of 1/50. The solution was incubated at 37 °C for 18 h, after which digestion was terminated by adding 0.5 vol of 5% formic acid. The products of digestion were desalted using a "Peptide Micro Trap" cartridge (Michrom BioResources) with elution in 80 μL of acetonitrile/water (80/20, v/v, incorporating 0.1% formic acid).

Mass Spectrometry. Mass spectrometric (MS) analysis of the partial trypsin digestion products was performed using a Micromass (Manchester, U.K.) Quattro tandem quadrupole mass spectrometer, upgraded to Quattro II specifications, equipped with an electrospray source. A portion of the eluate (10 μL) was introduced using a syringe driver (Harvard Apparatus, South Natick, MA) set to deliver a flow rate of 5 μL/min. The capillary potential was held between 3 and 4 kV, and the cone was set to 30−40 V. All potentials are reported relative to the skimmer. Electrospray mass spectra were recorded at a resolution set to give a peak width at half-height of 0.7 *m*/*z*-units for a monoisotopic peak of a singly charged ion. The *m*/*z* range 200−1600 was repetitively scanned at 14 s/scan. Spectra were acquired for two minutes under control of Masslynx software (Micromass) and were processed using the maximum entropy approach (*41*).

MS and tandem MS of complete trypsin digestion products were performed using a Micromass Q-ToF instrument equipped with an electrospray source. Initial MS screening of the digest mixture was carried out using a portion of the eluate (~5 μL) which was introduced using a syringe driver (Harvard Apparatus) set to deliver a flow rate of 0.5 μL/min. For tandem MS, a 1 μL portion of the eluate was

[1] Abbreviations: DTT, dithiothreitol; EDTA, ethylenediaminetetraacetic acid; ESI-MS, electrospray ionization mass spectrometry; *m*/*z*, mass/charge; MS, mass spectrometry; NMR, nuclear magnetic resonance; Tris, tris(hydroxymethyl)aminomethane.

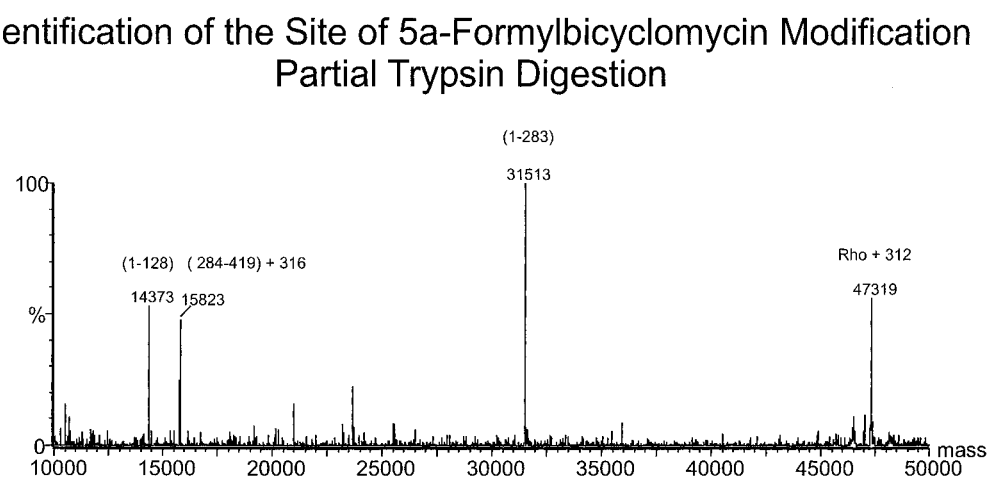

FIGURE 1: Mass spectrometric analysis of the partial trypsin hydrolysis product of **3**-modified rho. The spectrum shown was obtained by maximum entropy processing of the raw data which records the *m*/*z* ratios of multiply charged ions.

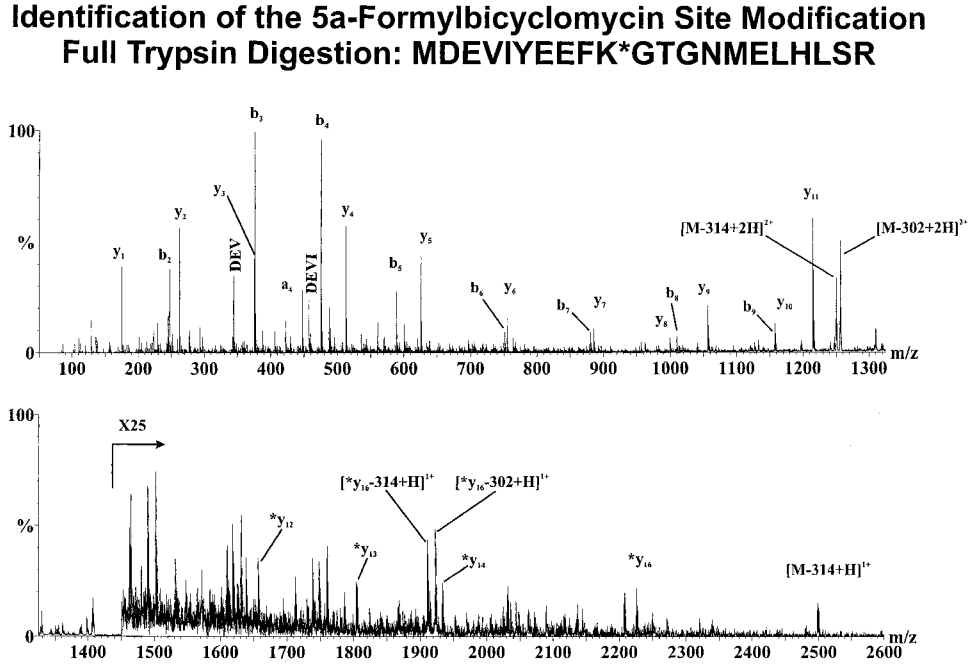

FIGURE 2: Tandem MS analysis of trypsin digest of **3**-modified rho. The spectrum shows product ions derived from precursors of *m*/*z* 1407 corresponding to $[M + 2H]^{2+}$ for the tryptic fragment comprising residues 327−347 and incorporating a modified K336. Fragment ions are labeled according to the nomenclature of Biemann (*42*). Fragments that are designated by an asterisk are designate ions modified by binding **3**.

introduced into a gold-coated borosilicate glass capillary with a 1 μm tapered tip (Micromass). To obtain the product ion spectrum (Figure 2), a doubly charged ion of *m*/*z* 1407.0 was selected as the precursor using a quadrupole resolution set to transmit a window of ± 2 *m*/*z*, and subjected to collisional activation, using a collision energy of 96−116 eV and an indicated (manifold) pressure of argon collision gas of 5×10^{-5} mbar. Fragment ions are labeled according to the nomenclature of Biemann (*42*).

RESULTS

Adduction of Rho by Bicyclomycin Derivative. As previously shown, inhibition of rho by **3** was competitive with bicyclomycin (*43*). The imine adduct derived from **3** was more stable than the corresponding imine obtained from 5a-(3-formylanilino)dihydrobicyclomycin (**2**) (*44*), and its stability was enhanced by adding ATP (ADP) (*43*). Treatment of the imine generated from **3** with $NaBH_4$ led to irreversible inhibition (*43*). Mass spectrometric data (*43*) suggested that five of the six subunits were labeled at a single site.

Localization of 3-Modified Rho. Partial trypsin-digested fragments from **3**-labeled rho were analyzed by MS. Partial trypsin hydrolysis of a fully **3**-modified rho amine sample containing poly C provided products corresponding to residues 1−128 (14 373 Da), 1−283 (31 513 Da), and 284−419 (15 823 Da) (Figure 1). The cleavage product incorporating residues 284−419 was displaced approximately 316 Da from the corresponding control partial trypsin experiment using wild-type rho (15 509 Da). Similar displacements were not observed for the other protein fragments. This finding localizes the lysine residue targeted by **3** to the C-terminus (Figure 1).

To identify the specific amino acid residue modified by **3,** mass spectrometric analysis was conducted on the un-

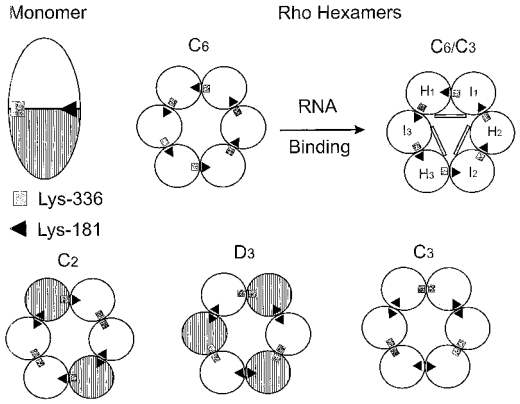

FIGURE 3: The possible symmetry models of the subunit arrangement for the hexameric rho protein. The top (N-terminal) half of rho is not hatched while the bottom (C-terminal) half is hatched. Data presented favor the C6/3 model of rho.

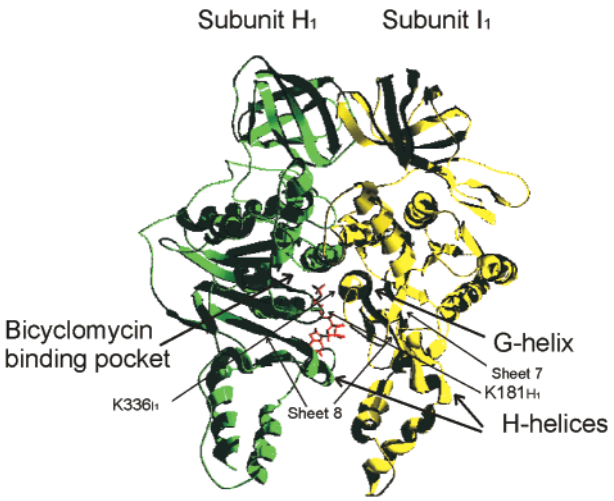

FIGURE 4: A model of the bicyclomycin binding pocket between the H_1 and I_1 monomers of rho. The model was built by threading the rho sequence on the F and B subunits of F_1-ATP synthase, which correspond to the tight-binding ATP β and α subunits, respectively. The model was created using Swiss pdbViewer (*46*) and energy minimized using INSIGHT II (MSI Inc.). The rendering was done using the POVRAY rendering package from output provided from Swiss pdbViewer.

fractionated mixture from the total trypsin digestion. Comparison of observed trypsin fragment masses with those predicted for unmodified rho showed a single component of the mass spectrum at *m*/*z* 1407**,** apparently corresponding to the $[M + 2H]^{2+}$ ion derived from the peptide incorporating residues 327−347 (MDEVIYEEFKGTGNMELHLSR) with modification of the lysine residue by reaction with **3**. Modification of K336 would be expected to abolish tryptic cleavage at this residue.

Tandem mass spectrometric analyses were performed to record the spectrum of product ions derived from *m*/*z* 1407.0 (Figure 2). C-Terminal (y-type) fragment ions, which retain the modified lysine residue, are accompanied by satellite ions arising by partial or complete loss (302 or 314 Da) of the derived bicyclomycin moiety. The data are in agreement with the proposed sequence, with modification of K336, and are therefore consistent with the results of the partial tryptic digestion analysis**.** The product ion spectrum of the triply charged ($[M + 3H]^{3+}$) analogue was also recorded and was similarly consistent with the proposed structure.

Covalent modification of K336 by **3** was difficult to reconcile based on a single subunit model of rho with previous data showing the covalent modification of K181 with **2** (*40*). From our previous model (*32*), the location of K336 lies on the opposite face from K181 of the single subunit model (Figure 3).

*Modeling of Rho and the Site of **3** Adduction*. A model of rho protein was generated to provide further understanding of the basis of K336 labeling by **3**. Accordingly, the rho sequence was threaded on the structure of the neighboring F and B subunits of bovine heart F_1-ATP synthase corresponding to the β subunit containing the catalytically bound ATP and the neighboring α subunit, respectively [nomenclature of Abrahams et al. (*45*)]. The derived rho structure is shown in Figure 4 where H_1 represents the F (β) and I_1 the B (α) subunit. The sequence threading was done using Swiss pdbViewer and submitted via the Internet for completion (*46*). Two gaps in the F subunit sequence required correcting when the rho sequence was threaded on the structure. The first gap corresponded to the absence of 13 amino acids in the F_1-ATP synthase sequence, compared with the rho sequence, between E226 and V227 at the loop junction between helix C and sheet 5. Residues V223 and V228 were constrained, and the program built several loops to close the gap. The lowest energetic conformer was chosen to fill the gap. This loop did not alter the internal sheet structure seen in F_1-ATP synthase. The second gap eliminated 38 residues from the F subunit of F_1-ATP synthase located between T383 and Q384 of the rho sequence and corresponds to the F_1-ATP synthase F subunit residues G364 through K401. This partially eliminated helices 1 and 2 at the C-terminal domain including the DELSEED sequence thought to interact with the γ subunit (*45*). A single gap on the I_1 subunit corresponding to the second gap on the H_1 subunit of rho between T383 and Q384 was corrected to fit the B subunit of F_1-ATP synthase eliminating residues R381−L417. The model was energy minimized using the Consistent Valence Force Field package included in the INSIGHT II/DISCOVER module (Biosym/Molecular Simulations Inc., San Diego, CA). Amino acid residues F355−D359 are speculated to be involved in ATP binding (*30*) and residues M393−E401 are consistent with the ATP binding domain near the adenosine binding site of F_1-ATP synthase (*45*), suggesting that gap closure at residue T383 did not alter the ATP binding site in the rho model.

The rho structural model revealed that K336 (the site of **3**-modification) on the G helix of the I_1 subunit lay 5 Å from K181 [the site of **2**-modification (*40*)] at the P loop near the B and D helices on the H_1 subunit (Figure 4). Thus, **1** binding pocket at the H_1 subunit may extend across the interface to the I_1 subunit. This is consistent with the location of the G337S mutation leading to **1** resistance (*38*). We saw no cross labeling of K181 with **3** or labeling of K336 with **2**. The specificity for each residue to be labeled uniquely is somewhat surprising. The bicyclomycin derivative **2** is four bonds longer than **3** and upon binding to rho the formylanilino group may bend closer to K181 while the shorter **3** would interact with K336 without hindrance.

Our model indicates that **1** binding occurs near the ATP hydrolysis pocket and is proximal to an adjacent subunit. It imposes an overall C6 subunit symmetry on the rho hexamer and excludes hexameric D3 symmetry. The structural

similarity of rho to F_1-ATP synthase suggests that a mechanistic equivalence exists among a class of hexameric ATP utilizing enzymes that include *E. coli* DnaB, T7 helicase, rho, and F_1-ATP synthase (*47*). Studies have shown that rho has at least three high affinity ATP binding sites (*24*, *25*) while other studies have shown that besides the three high affinity sites rho also has three low ATP affinity sites (*27*, *48*). Recently, rapid kinetics experiments suggest the tight ATP binding sites are noncatalytic (inactive), I_n, and the weak ATP binding sites are catalytic (hydrolytic), H_n, (*26*). On the basis of noncatalytic, I_n, and catalytic, H_n ATP binding subunits, and the binding of **1** to rho, an overall C6/C3 symmetry is proposed for rho (Figure 3).

DISCUSSION

The mechanism of F_1-ATP synthase requires ATP synthesis sites located on the three β subunits to alternate in the structure with noncatalytic (nonreleasable) ATP binding α subunits. Rotary motion of the γ subunit in the central hole of the toroid leads to ATP synthesis on the β subunits which alternate between a tight ATP binding site, a loose ADP and P_i binding site, and an empty site (*45*, *49*, *50*). On the other hand, F_1-ATP synthase mediated hydrolysis of ATP drives a rotary motion of the γ subunit in a process that is the reverse of ATP synthesis (*49*−*51*). Rho has no protein equivalent to the γ subunit, but it has been proposed that RNA binding within the central hole at the secondary binding site is required for ATP hydrolysis coupled to RNA translocation (*31*). Bicyclomycin prevents the hydrolysis of ATP and slows down RNA tracking toward the stalled polymerase (*23*, *37*, *38*). The location of bicyclomycin binding on the rho model suggests a mechanism for bicyclomycin inhibition of rho and hints at a mechanism of rho tracking. This model includes alternating catalytic and noncatalytic ATP binding subunits (*25*, *26*, *52*) and the sequential hydrolysis of ATP coupled with RNA binding to the secondary tracking site.

Our model contains two hypotheses. First, that binding of individual rho subunits into dimers leads to local alterations in the ATP binding site giving rise to a tight (noncatalytic) site and a weak (catalytic) ATP site and, second, after RNA *rut* recognition at the primary binding site, RNA then binds to a secondary site at one of three interfaces between the active and inactive subunits and activates ATP hydrolysis. In our model, we speculate that the 5′ RNA end is closest to the primary binding site (residues 1−130) of the H_1 subunit, and the 3′ RNA end is nearest the C-terminus of the I_1 subunit in the rho model. ATP hydrolysis drives RNA binding counterclockwise (rho clockwise) from one catalytic site to another. Bicyclomycin binds near or at the catalytic hydrolysis site, and by analogy to F_1-ATP synthase, close to the bound magnesium and water thought to be involved in catalysis (*45*), thus preventing the conversion of ATP to ADP and P_i. We have shown that bicyclomycin derivative binds to 5 of the 6 subunits (*43*), however, the model predicts that three bicyclomycins would be required for complete inhibition of ATP hydrolysis and possibly fewer if ATP hydrolysis were required for RNA translocation to activate the next hydrolysis site.

Long-range interactions between subunits are required to cause degeneration of the C6 symmetry to C6/C3 and the formation of catalytic (H) and noncatalytic (I) subunits. These

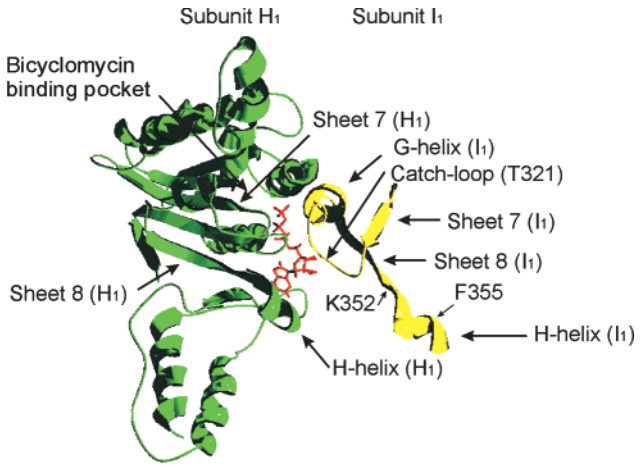

FIGURE 5: Model of the sheet 7-G-helix-sheet 8 section of one rho subunit (subunit I_1) interaction with the ATP hydrolysis domain of the active subunit (subunit H_1). ATP is shown bound to only the H_1 subunit. The bicyclomycin binding pocket has been previously proposed (*32*).

interactions must arise at the subunit−subunit interface, and we speculate that the G helix is involved in this long-range subunit interaction. The G helix is the site of mutations implicated with the secondary RNA (tracking) site (*30*, *36*) and K336, which is covalently modified by **3**, lies in the middle of this helix. The ATP hydrolysis site on the H_1 subunit must lie very close to the G helix of the neighboring I_1 subunit since **3** binds near the H_1 subunit ATP hydrolysis site and competes with **1** for binding yet labels the G helix (residue K336). The relative locations of K336 on the I_1 subunit and K181 on the H_1 subunit at or near the **1** binding site are consistent with proposed C6/C3 symmetry of rho (Figure 3). Amino acids prior to the G helix, residues 311−317, sheet 7, are highly conserved among rho sequences; they constitute part of the ATP binding site near the terminal phosphate. Sheet 7 labeled in Figure 5 shows its position in the I_1 subunit, however, ATP is not shown bound to this subunit. The corresponding sheet 7 in the H_1 subunit is labeled as such. Residues after the G helix on the I_1 subunit make up part of the adenosine binding pocket on the I_1 subunit. This connection allows a direct link between ATP hydrolysis on the H_1 subunit and ATP binding on the I_1 subunit. Figure 5 depicts the location of the G helix in the I_1 subunit with respect to the ATP hydrolysis site on the H_1 subunit. It is important to note that the distinction between the H and I subunits arises only after RNA binds to the secondary (tracking) site; no ATP hydrolysis occurs when RNA is omitted. This suggests that RNA binding on the H_1 subunits is different from RNA binding on the I_1 subunits. This differential binding promotes ATP hydrolysis on the H_1 subunit and tight, noncatalytic, ATP-binding on the I_1 subunit. The differential G helix conformations and RNA secondary binding properties of the H_1 and I_1 subunits lead to rho C6/C3 symmetry and function.

Our model brings together previous experimental information concerning the location of the secondary site of RNA binding. Rho residues 318−325 correspond to the catch loop in F_1-ATP synthase (residues 309−316 of the β subunit) that is thought to interact directly with the γ subunit. By analogy, this loop is believed to interact with RNA at the secondary site. This notion is reinforced by the finding that rho mutant

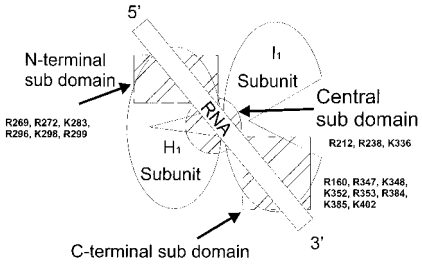

FIGURE 6: Diagrammatic representation of RNA tracking along rho using the different subdomain RNA binding sites. The hashed squares are the N-terminal and C-terminal RNA binding subdomains and the circle represents the central RNA binding subdomain.

T323I affects the secondary RNA binding site (*30*) (Figure 5). Sheet 8 (residues 340−345) and helix H (residues 347−354) are contiguous with F355, which is in close contact with and lies parallel to the adenosine ring in the ATP binding pocket. The mutation, K352E (*36*) (see Figure 5), was shown to affect the secondary RNA binding site and is one of four nearly completely conserved positive residues among rho proteins (R347, K348, K352, R353) joining the G helix with the adenosine binding pocket. RNA binding at or near sheet 8−helix H on the I_1 subunit could inhibit ATP hydrolysis and increase the K_d for ATP at the I_1 binding sites. However, RNA binding to the H_1 subunits activates ATP hydrolysis. Reason suggests that RNA binds to the H_1 subunit at a locus different from the I_1 subunit. Rho residues R269, R272, K283, R296, K298, and R299 cluster near the top of the ATP binding domain on the H_1 subunit while the previously mentioned sheet 8 lies at the C-terminal part of the ATP binding domain of the I_1 subunit. Amino acid residues in this locus include R347, K348, K352, and R353. The three-dimensional model indicates additional proximal, positively charged residues R160, R384, K385, and K402. Figure 6 shows the RNA lying across the H_1-I_1 subunit interface and across the ATP hydrolysis pocket of the H_1 subunit and binding with both patches of positively charged residues. Further inspection of the model indicates that there are several lysine residues (K212, R238, K336) near the ATP hydrolysis site opposite the protein hinge (see description below). These three sets of lysine and arginine rich sites could form a strip of positive charge in the central hole of rho. We suspect that these may bind to the RNA phosphate backbone and mediate RNA tracking toward the polymerase.

The apparent close correspondence of the F_1-ATP synthase and the rho structures has prompted us to consider whether this similarity extends to the mechanism. Central to our reasoning is the assumption that the RNA chain behaves similar to the γ subunit of F_1-ATP synthase. ATP hydrolysis has been shown to rotate the γ subunit (*51*), suggesting that the hydrolysis could lead to conformational changes. We suggest that rho advances along the RNA powered by an analogous conformational change.

Several possible mechanisms could allow rho progression along the RNA chain via successive binding to alternating, secondary RNA binding sites (domains). One appealing model is the "wobble inch-worm" -like mechanism depicted in Figure 7. This mechanism takes advantage of the apparent large cleft in the rho H_1 subunit model, similar to a feature in F_1-ATP synthase (*45*, *53*), between the P-loop residues (*175*−*188*), sheet 7, and helix B on the bottom and sheet 6 and helix C on the top. This divides the ATP hydrolysis

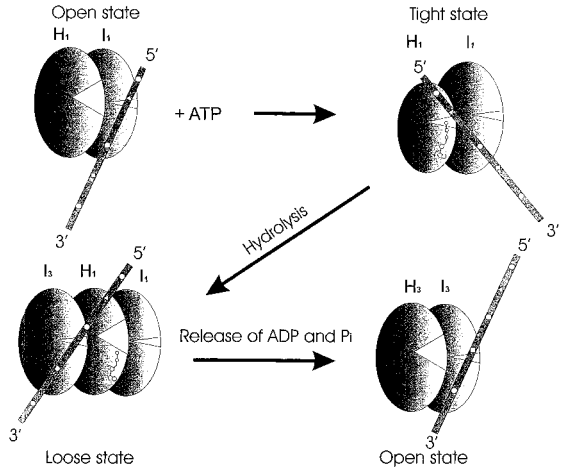

FIGURE 7: The proposed dimeric interaction between RNA and the H and I subunits depicting the "wobble inch-worm"-like tracking mechanism. Bicyclomycin binding at the hydrolysis pocket would prevent RNA tracking and inhibit ATP hydrolysis. In this model, the RNA is moving in relationship to rho; a more accurate representation would be RNA remaining vertical and rho protein wobbling as it moves 5′ to 3′ down the RNA.

pocket between two globular domains connected with a hinge region consisting of residues 149−152, 198−201, 256−259, and 308−310. It has been shown that the F_1-ATP synthase β subunit has a conformation in which these domains are separated when the cleft is vacant and closed upon ATP binding and hydrolysis (*45*, *53*). H and I dimers are labeled with subscripts to denote different dimer pairs within the hexamer. In our model (Figure 7), RNA first binds preferentially to the I_1 subunit of the rho secondary site prior to ATP binding on the H_1 subunit. ATP binding closes the cleft, allowing RNA to bind at the top of the H_1 subunit and trigger ATP hydrolysis. ATP hydrolysis causes the cleft to open, driving rho along the RNA. Concomitantly, RNA is released from the I_1 subunit. Loss of ADP and P_i allows rho to relax back to the initial state where RNA binding occurs to the I_3 subunit. As rho carries out this catalytic cycle, RNA binds sequentially between the H_n and the I_n subunits moving in a counterclockwise manner at one of three ATP catalytic interfaces. This model also predicts that RNA must have a structure that permits multiple interactions with the rho toroid. The "wobble inch-worm" model envisions wobbling of rho as RNA binds from one site to another, allowing tracking without twisting or rotation of the RNA. Further experimentation will be required to test these notions and to provide additional details.

ACKNOWLEDGMENT

We thank Dr. M. Kawamura and the Fujisawa Pharmaceutical Co., Ltd., Japan, for the gift of bicyclomycin, Dr. T. Platt (University of Rochester) for the rho overproducing strain of *E. coli*, Dr. James Briggs and Gabriela Mustata (University of Houston) for their help in energy minimizing the threaded rho model.

REFERENCES

1. von Hippel, P. H., Yager, T. D., Bear, D. G., McSwiggen, J. A., Geiselmann, J., Gill, S. C., Linn, J. D., and Morgan, W. D. (1987) in *RNA polymerase and the regulation of transcription* (Rernlkoff, W. S., Ed.) pp 325−334, Elsevier Science Publications.

2. Chen, C.-Y. A., and Richardson, J. P. (1987) *J. Biol. Chem. 262*, 11292−11299.
3. Platt, T., and Richardson, J. P. (1992) in *Transcriptional regulation* (McKnight, S. L., and Yamamoto, K. R., Eds.) pp 365−368, Cold Spring Harbor Laboratory Press, Plainview, NY.
4. Platt, T. (1994) *Mol. Microbiol. 11*, 983−990.
5. Das, A., Court, D., and Adhya, S. (1976) *Proc. Natl. Acad. Sci. U.S.A. 73*, 1959−1963.
6. Inoko, H., Shigesada, K., and Imai, M. (1977) *Proc. Natl. Acad. Sci. U.S.A. 74*, 1163−1166.
7. Richardson, J. P., and Carey, J. L., III (1982) *J. Biol. Chem. 257*, 5767−5771.
8. Pinkham, J. L., and Platt, T. (1983) *Nucleic Acids Res.* 3531−3545.
9. Bear, D. G., Hicks, P. S., Escudero, K. W., Andrews, C. L., McSwiggen, J. A., and von Hippel, P. H. (1988) *J. Mol. Biol. 199*, 623−635.
10. Oda, T., and Takanami, M. (1972) *J. Mol. Biol. 71*, 799−802.
11. Knopf, K.-W., and Bujard, H. (1975) *Eur. J. Biochem. 53*, 371−385.
12. Geiselmann, J., Wang, Y., Seifried, S. E., and von Hippel, P. H. (1993) *Proc. Natl. Acad. Sci. U.S.A. 90*, 7754−7758.
13. Horiguchi, T., Miwa, Y., and Shigesada, K. (1997) *J. Mol. Biol. 269*, 514−528.
14. Martinez, A., Burns, C. M., and Richardson, J. P. (1996) *J. Mol. Biol. 257*, 909−918.
15. Richardson, J. P., and Ruteshouser, E. C. (1986) *J. Mol. Biol. 189*, 413−419.
16. Morgan, W. D., Bear, D. G., and von Hippel, P. H. (1983) *J. Biol. Chem. 258*, 9553−9564.
17. McSwiggen, J. A., Bear, D. G., and von Hippel, P. H. (1988) *J. Mol. Biol. 199*, 609−622.
18. Gan, E., and Richardson, J. P. (1999) *Biochemistry 38*, 16882−16888.
19. Galluppi, G. R., and Richardson, J. P. (1980) *J. Mol. Biol. 138*, 513−539.
20. Richardson, J. P. (1982) *J. Biol. Chem. 257*, 5760−5766.
21. Brennan, C. A., Dombroski, A. J., and Platt, T. (1987) *Cell 48*, 945−952.
22. Jin, D. J., Burgess, R. R., Richardson, J. P., and Gross, C. A. (1992) *Proc. Natl. Acad. Sci. U.S.A. 89*, 1453−1457.
23. Magyar, A., Zhang, X., Kohn, H., and Widger, W. R. (1996) *J. Biol. Chem. 271*, 25369−25374.
24. Stitt, B. L. (1988) *J. Biol. Chem. 263*, 11130−11137.
25. Stitt, B. L., and Xu, Y. (1998) *J. Biol. Chem. 373*, 26477−26486.
26. Kim, D. E., Shigesada, K., and Patel, S. S. (1999) *J. Biol. Chem. 274*, 11623−11628.
27. Geiselmann, J., and von Hippel, P. H. (1992) *Protein Sci.* 850−860.
28. Geiselmann, J., Seifreid, S. E., Yager, T. D., Liang, C., and von Hippel, P. H. (1992) *Biochemistry 31*, 121−132.
29. Dombroski, A. J., LaDine, J. R., Cross, R. L., and Platt, T. (1988) *J. Biol. Chem. 263*, 18810−18815.
30. Miwa, Y., Horiguchi, T., and Shigesada, K. (1995) *J. Mol. Biol. 254*, 815−837.
31. Richardson, J. P. (1996) *J. Biol. Chem. 271*, 1251−1254.
32. Magyar, A., Zhang, X., Abdi, F., Kohn, H., and Widger, W. R. (1999) *J. Biol. Chem. 274*, 7316−7324.
33. Brennan, C. A., and Platt, T. (1991) *J. Biol. Chem. 266*, 17296−17305.
34. Allison, T. J., Wood, T. C., Briercheck, D. M., Rastinejad, F., Richardson, J. P., and Rule, G. S. (1998) *Nat. Struct. Biol. 5*, 352−356.
35. Briercheck, D. M., Wood, T. C., Allison, T. J., Richardson, J. P., and Rule, G. S. (1998) *Nat. Struct. Biol. 5*, 393−399.
36. Pereira, S., and Platt, T. (1995) *J. Mol. Biol. 251*, 30−40.
37. Park, H., Zhang, X., Moon, H., Zwiefka, A., Cox, K., Gaskell, S. J., Widger, W. R., and Kohn, H. (1995) *Arch. Biochem. Biophys. 323*, 447−454.
38. Zwiefka, A., Kohn, H., and Widger, W. R. (1993) *Biochemistry 32*, 3564−3570.
39. Nowatzke, W. L., Keller, E., Koch, G., and Richardson, J. P. (1997) *J. Bacteriol. 179*, 5238−5240.
40. Riba, I., Gaskell, S. J., Cho, H., Widger, W. R., and Kohn, H. (1998) *J. Biol. Chem. 273*, 34033−34041.
41. Ferrige, A. G., Seddon, M. J., and Jarvis, S. (1991) *Rapid Commun. Mass Spectrom. 5*, 374−379.
42. Biemann, K. (1988) *Biomed. Environ. Mass Spectrom. 16*, 95−111.
43. Vincent, F., Widger, W. R., Openshaw, M., Gaskell, S. J., and Kohn, H. (2000) 5a-Formylbicyclomycin: Studies on the bicyclomycin-rho interaction. *Biochemistry 39*, 9067−9076.
44. Cho, H., Park, H., Zhang, X., Riba, I., Gaskell, S. J., Widger, W. R., and Kohn, H. (1997) *J. Org. Chem. 62*, 5432−5440.
45. Abrahams, J. P., Leslie, A. G., Lutter, R., and Walker, J. E. (1994) *Nature 370*, 621−628.
46. Guex, N., and Peitsch, M. C. (1997) *Electrophoresis 18*, 2714−2723.
47. Lohman, T. M., and Bjornson, K. P. (1996) *Annu. Rev. Biochem. 65*, 169−214.
48. Seifreid, S. E., Easton, J. B., and von Hippel, P. H. (1992) *Proc. Natl. Acad. Sci. U.S.A. 89*, 10454−10458.
49. Walker, J. E. (1998) *Angew. Chem., Int. Ed. 37*, 2308−2319.
50. Boyer, P. D. (1998) *Angew. Chem., Int. Ed. 37*, 2297−2307.
51. Noji, H., Yasuda, R., Yoshida, M., and Kinosita, K. (1997) *Nature 386*, 299−302.
52. Kim, D. E., and Patel, S. S. (1999) *J. Biol. Chem. 274*, 32667−32671.
53. Allison, W. (1998) *Acc. Chem. Res. 31*, 819−826.

BI000504+